Unstructured-mesh based non-oscillatory-forward-in-time integration for atmospheric flows

J. Szmelter

Loughborough University, UK

Acknowledgements: Mike Gillard , Francesco Cocetta, Piotr Smolarkiewicz

Funded by the European Union

Generalised Nonhydrostatic Model

Smolarkiewicz et. al. JCP 2016

$$\frac{\partial \mathcal{G}\varrho}{\partial t} + \nabla \cdot (\mathcal{G}\varrho \boldsymbol{v}) = 0$$

$$\frac{\partial \mathcal{G}\varrho\theta'}{\partial t} + \nabla \cdot (\mathcal{G}\varrho \boldsymbol{v}\theta') = -\mathcal{G}\varrho \left(\tilde{G}^T \boldsymbol{u} \cdot \nabla\theta_a - \mathcal{H}\right)$$

$$\frac{\partial \mathcal{G}\varrho \boldsymbol{u}}{\partial t} + \nabla \cdot (\mathcal{G}\varrho \boldsymbol{v} \otimes \boldsymbol{u}) = -\mathcal{G}\varrho \left(\Theta \tilde{G} \nabla\varphi + g\Upsilon_B \frac{\theta'}{\theta_b} + \boldsymbol{f} \times (\boldsymbol{u} - \Upsilon_C \boldsymbol{u}_a) - \mathcal{M}'(\boldsymbol{u}, \boldsymbol{u}, \Upsilon_C) - \boldsymbol{\mathcal{D}}\right)$$

$$\varrho := \left[\rho(\boldsymbol{x},t), \frac{\rho_b(z)\theta_b(z)}{\theta(\boldsymbol{x},t)}, \rho_b(z)\right] \quad \varphi := [c_p\theta_0\pi', c_p\theta_0\pi, c_p\theta_b\pi] \quad \Theta := \left[\frac{\theta}{\theta_0}, \frac{\theta}{\theta_0}, 1\right] \quad \Upsilon_B := \left[\frac{\theta_b(z)}{\theta_a(\boldsymbol{x})}, \frac{\theta_b(z)}{\theta_a(\boldsymbol{x})}, 1\right] \quad \Upsilon_C := \left[\frac{\theta}{\theta_a(\boldsymbol{x})}, \frac{\theta}{\theta_a(\boldsymbol{x})}, 1\right]$$

$$[compressible, pseudo\text{-}incompressible, anelastic]$$

$$\varphi = c_p\theta_0 \left[\left(\frac{R_d}{p_0}\rho\theta\right)^{R_d/c_v} - \pi_a\right].$$

Ideal gas law for compressible option

NFT based Nonhydrostatic Models

Non-oscillatory Forward-in-Time (NFT)

$$\frac{\partial G\Phi}{\partial t} + \nabla \cdot (\boldsymbol{V}\Phi) = G\mathcal{R}$$

$$\Phi_i^{n+1} = \mathcal{A}_i\left(\Phi^n + \tfrac{1}{2}\delta t\mathcal{R}, \boldsymbol{V}^{n+\frac{1}{2}}, G^n, G^{n+1}\right) + \tfrac{1}{2}\delta t\mathcal{R}^{n+1}$$

- Semi-implicit
- Multidimensional Positive Definite Advection Transport Algorithm (MPDATA)
- Krylov solver

For details see:
Kühnlein et. al. GMD 2019 for global model (compressible) FVM (Finite Volume Module) of IFS
Szmelter et. al. JCP 2019 for local model (anelastic)

Global flows - FVM: discrete operators

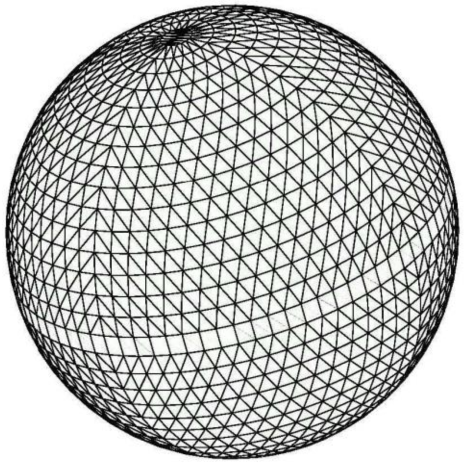

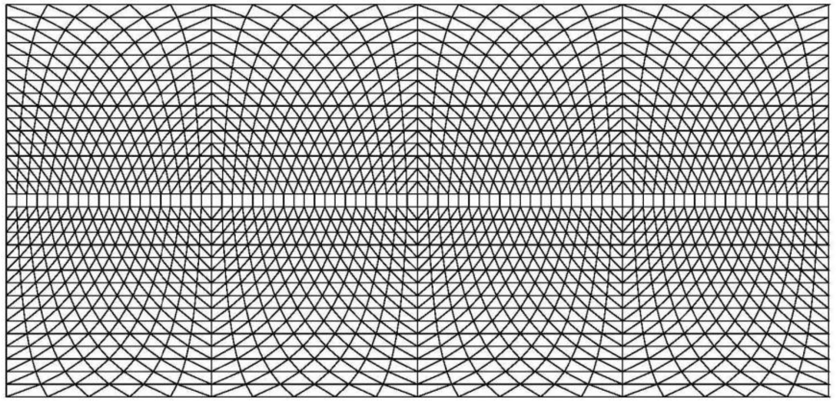

Periodic boundaries

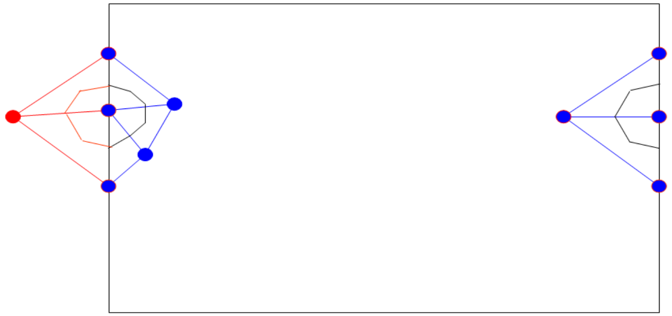

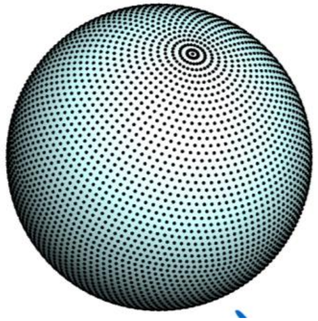

Octahedral mesh

IFS grid

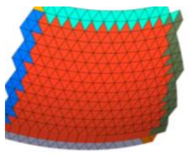

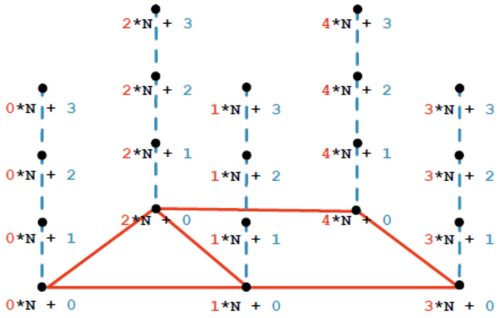

$$\int_{\Omega} \nabla \cdot \mathbf{A} = \int_{\partial\Omega} \mathbf{A} \cdot \mathbf{n} = \frac{1}{\mathcal{V}_i} \sum_{j=1}^{l(i)} A_j^{\perp} S_j$$

dual volume: $\mathcal{V}_i$, face area: S_j

Uses a co-located data arrangement for all prognostic variables

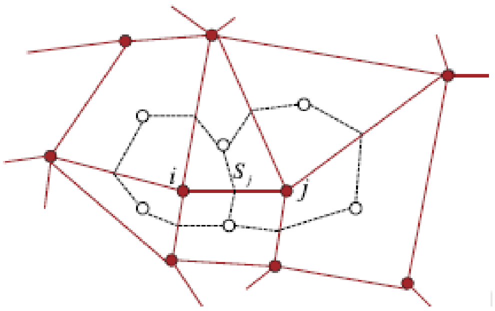

Pole treatment

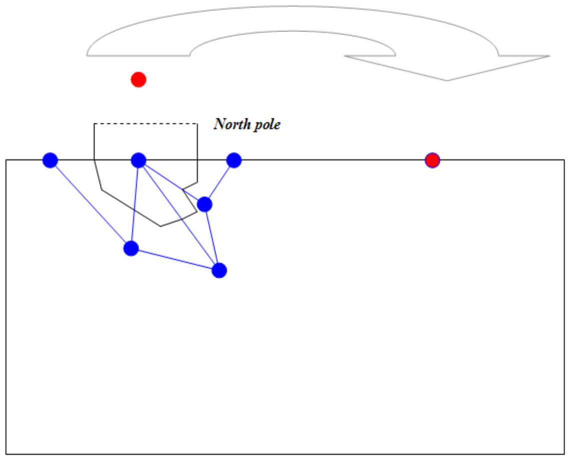

Szmelter & Smolarkiewicz JCP 2010

Deconinck et. al. *Parallel Proc &Appl Math 2016*

Generalised Conjugate Residual (k) scheme

Smolarkiewicz & Margolin 2000

$$\sum_{I=1}^{M}\frac{\partial}{\partial x^I}\left(\sum_{J=1}^{M}C^{IJ}\frac{\partial\phi}{\partial x^J}+D^I\phi\right)-A\phi=R$$

$$\mathcal{L}(\phi)-R=0\ .$$

$$\frac{\partial^k\mathcal{P}(\phi)}{\partial\tau^k}+\frac{1}{T_{k-1}(\tau)}\frac{\partial^{k-1}\mathcal{P}(\phi)}{\partial\tau^{k-1}}+...+\frac{1}{T_1(\tau)}\frac{\partial\mathcal{P}(\phi)}{\partial\tau}=\mathcal{L}(\phi)-R$$

For any initial guess, ϕ^0, set $r^0=\mathcal{L}\left(\phi^0\right)-R$, $p^0=\mathcal{P}^{-1}\left(r^0\right)$; then iterate:

For $n=1,2,...$ until convergence

for $\nu=0,...,k-1$

$$\beta=-\frac{\langle r^\nu\mathcal{L}\left(p^\nu\right)\rangle}{\langle\mathcal{L}\left(p^\nu\right)\mathcal{L}\left(p^\nu\right)\rangle},$$

$$\phi^{\nu+1}=\phi^\nu+\beta p^\nu,$$

$$r^{\nu+1}=r^\nu+\beta\mathcal{L}\left(p^\nu\right),$$

exit if $\|r^{\nu+1}\|\le\epsilon$,

$e=\mathcal{P}^{-1}\left(r^{\nu+1}\right)$,

evaluate $\mathcal{L}(e)$

for $l=0,..\nu$

$$\alpha_l=\frac{\langle\mathcal{L}(e)\mathcal{L}\left(p^l\right)\rangle}{\langle\mathcal{L}\left(p^l\right)\mathcal{L}\left(p^l\right)\rangle},$$

$$p^{\nu+1}=e+\sum_l^\nu\alpha_l p^l,$$

$$\mathcal{L}\left(p^{\nu+1}\right)=\mathcal{L}(e)+\sum_l^\nu\alpha_l\mathcal{L}\left(e^l\right),$$

reset $[\phi,r,e,\mathcal{L}(e)]^k$ to $[\phi,r,e,\mathcal{L}(e)]^0$

Richardson iteration

Take an operator $\mathcal{P} \approx \mathcal{L}$

$$\sum_{I=1}^{M} \frac{\partial}{\partial x^I} \left(\sum_{J=1}^{M} C^{IJ} \frac{\partial \phi}{\partial x^J} + D^I \phi \right) - A\phi = R$$

by neglecting cross derivative terms i.e. $I \neq J$

Solve the resulting residual equation:

$$\frac{\partial e}{\partial \tilde{\tau}} = \mathcal{P}(e) - r \quad \Rightarrow \quad e^{\mu+1} = e^{\mu} + \Delta\tilde{\tau} \left[\mathcal{P}(e^{\mu}) - r^{\nu+1} \right]$$

Due to the thin shell atmosphere: treat the unstructured horizontal direction explicitly and the structured vertical direction implicitly, i.e.

$$\text{let} \quad \mathcal{P}(e) \equiv \mathcal{P}_H(e^{\mu}) + \mathcal{P}_z(e^{\mu+1})$$

$$(I - \Delta\tilde{\tau}\mathcal{P}_z)\, e^{\mu+1} = e^{\mu} + \Delta\tilde{\tau} \left(\mathcal{P}_H(e^{\mu}) - r^{\nu+1} \right) = \mathcal{R}^{\mu}$$

$$e^{\mu+1} = \left[I - \Delta\tilde{\tau}\mathcal{P}_z \right]^{-1} \mathcal{R}^{\mu}$$

Use Thomas Algorithm

Smolarkiewicz & Margolin 2000

Unstructured mesh Jacobi iteration

$$\mathcal{P}(e) = r$$

$$\mathcal{P}(e) + \mathcal{D}(e) - \mathcal{D}(e) = r$$

Solve the residual equation by lagging the off-diagonal $\mathcal{P}$ components:

$$e^{\mu+1} = e^{\mu} - \frac{\mathcal{P}(e^{\mu}) - r^{\nu+1}}{\mathcal{D}}$$

Apply the thin shell atmosphere treatment again:

$$\text{let} \quad \mathcal{P}(e) \equiv \mathcal{P}_H(e^{\mu}) + \mathcal{P}_z(e^{\mu+1})$$

For the Helmholtz $0 = -\sum_{\ell=1}^{3} \left(\frac{A_\ell^\star}{\zeta_\ell} \nabla \cdot \zeta_\ell \tilde{\mathbf{G}}^T (\check{\mathbf{u}} - \mathbf{C} \nabla \varphi') \right) - B^\star (\varphi' - \widehat{\varphi}')$

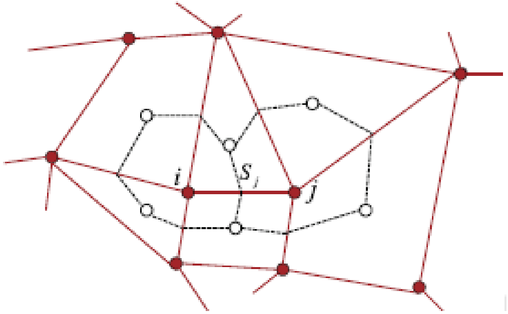

$$\mathcal{D}_{k,i} = -\frac{1}{4V_i} \sum_{l} \frac{A^\star_{l\,k,i}}{\zeta_{l\,k,i}} \sum_{j=1}^{nbrs} \frac{\zeta_{l\,k,j}}{V_j} \left(\mathcal{S}^2_{x\,j} (\tilde{\mathbf{G}}^T \mathbf{C})_{xx\,k,j} + \mathcal{S}^2_{y\,j} (\tilde{\mathbf{G}}^T \mathbf{C})_{yy\,k,j} \right)$$

$$\left(I + \frac{\mathcal{P}_z}{\mathcal{D}} \right) \hat{e}^{\mu+1} = e^{\mu} - \frac{\mathcal{P}_H(e^{\mu}) - r^{\nu+1}}{\mathcal{D}} \equiv \frac{\mathcal{R}^{\mu}}{\mathcal{D}}$$

$$\hat{e}^{\mu+1} = [\mathcal{D} + \mathcal{P}_z]^{-1} \mathcal{R}^{\mu}$$

Use Thomas Algorithm

Jacobi requires some solution relaxation:

$$e^{\mu+1} = (1-\omega)\, e^{\mu} + \omega \hat{e}^{\mu+1} \,, \quad \omega \approx \tfrac{2}{3}$$

Dry baroclinic instability, O360 mesh, Jacobi (left), Richardson (centre), Difference (right)

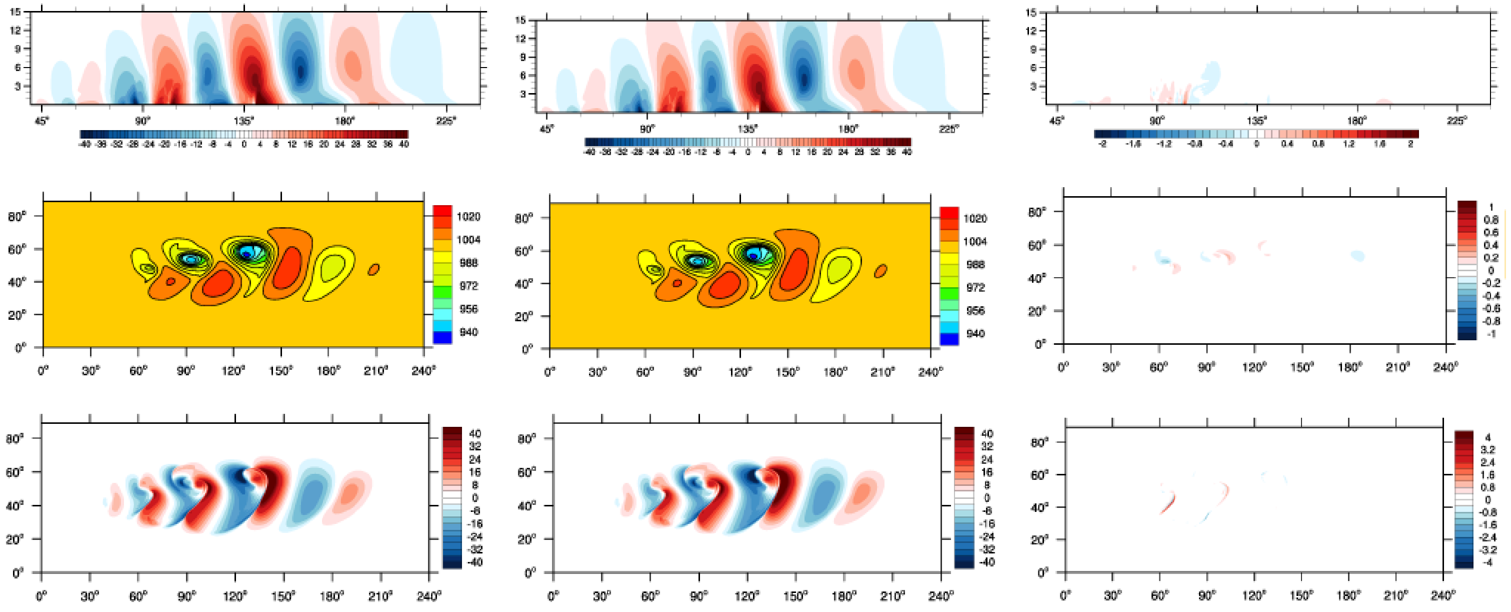

Vertical velocity at 53º N latitude

Upper Hemisphere
surface pressure

Upper Hemisphere
surface meridionial velocity

Table 1: 10 days, dry baroclinic instability test with 60 vertical levels, computed on the Cray XC30 at ECMWF (Dynamical core only).

Grid	Richardson runtime	Richardson convergence	Jacobi runtime	Jacobi convergence	Tasks x Threads	Total cores
O180	2897 s	14	1540 s	1	36 x 1	36
O360	3700 s	22	1374 s	1	108 x 6	648
O720	11296 s	33	3194 s	2	360 x 6	2160
O1280	35884 s	47	7976 s	2	720 x 6	4320
O1800	46670 s	56	8675 s	2	2400 x 6	14400

Jacobi provides ca 2x acceleration on coarse meshes expanding to ca 5-6 x acceleration on finer meshes

Preconditioners use 3 iterations

Unstructured mesh multigrid preconditioner in the horizontal

Parallel restriction, prolongation and Atlas mesh

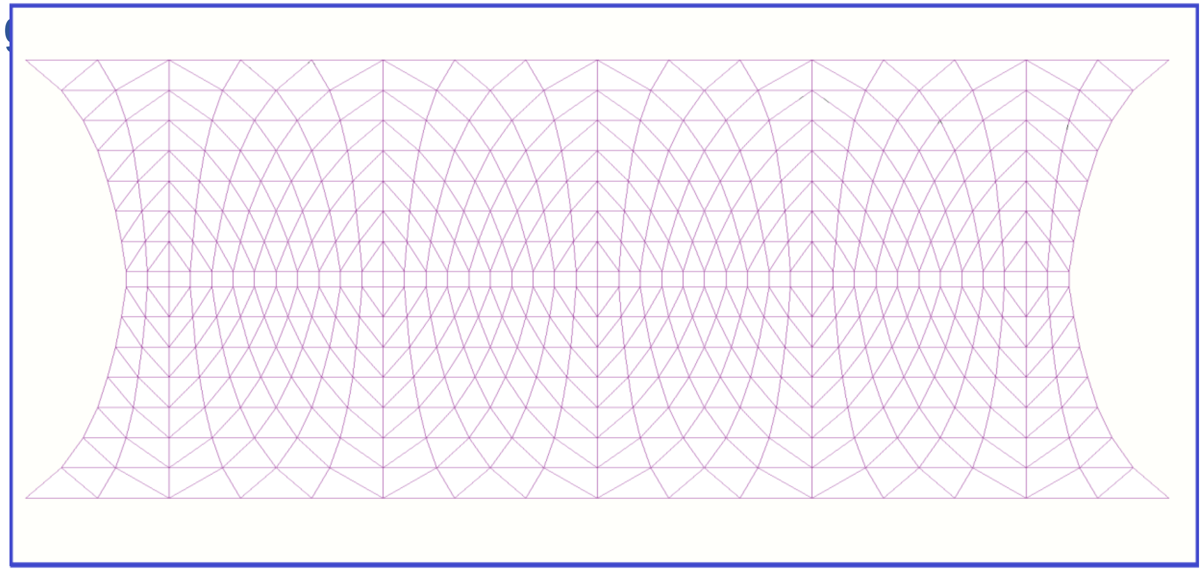

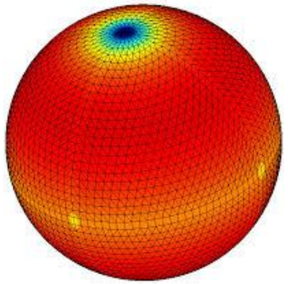

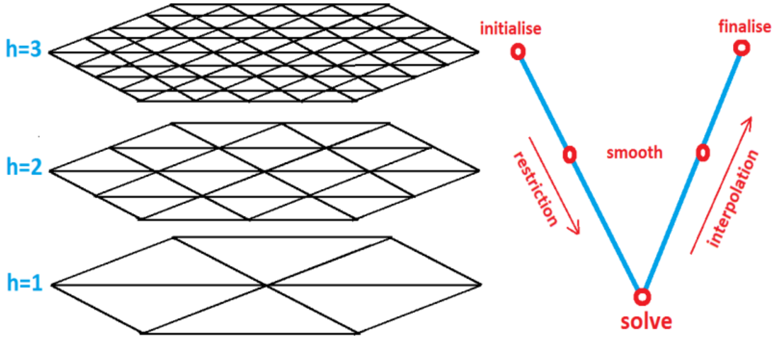

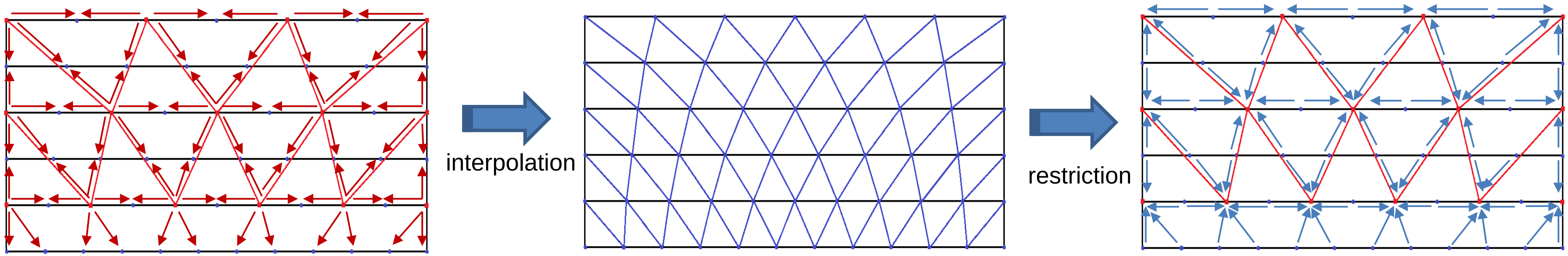

Coarse mesh | Fine mesh | Coarse mesh

Baroclinic Instability Testcase

O360 plots for day 10 of dry baroclinic instability test: Multigrid (top), Difference vs. Richardson (bottom).

vertical velocity at the 53º N;

Upper Hemisphere surface Pressure

Upper Hemisphere surface meridional velocity

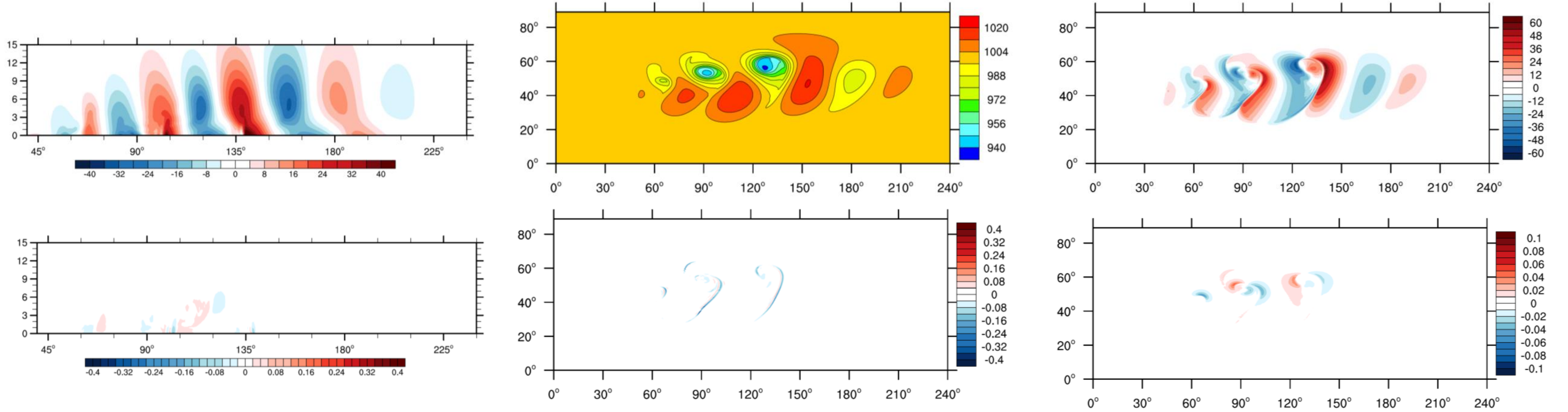

Grid	Richardson	Multigrid	Speedup	Task x thread
O360	814 s	403 s	2.02x	108 x 6 (648 cores)
O720	3001 s	1017 s	2.95x	360 x 6 (2160 cores)
O1280	13586 s	3038 s	4.41x	720 x 6 (4320 cores)
O1800	19544 s	4060 s	4.81x	2400 x 6 (14400 cores)

3 iterations

1 Jacobi as a smoother and 3 Jacobi on the coarse grid

10 days, dry baroclinic instability test ~27km Horizontal resolution, with 31 vertically stretched levels at a depth of 45km computed on the Cray XC30 at ECMWF (Dynamical core only)

Local models: The effect of critical levels on stratified flows past an axisymmetric mountain

Szmelter et. al. JCP 2015

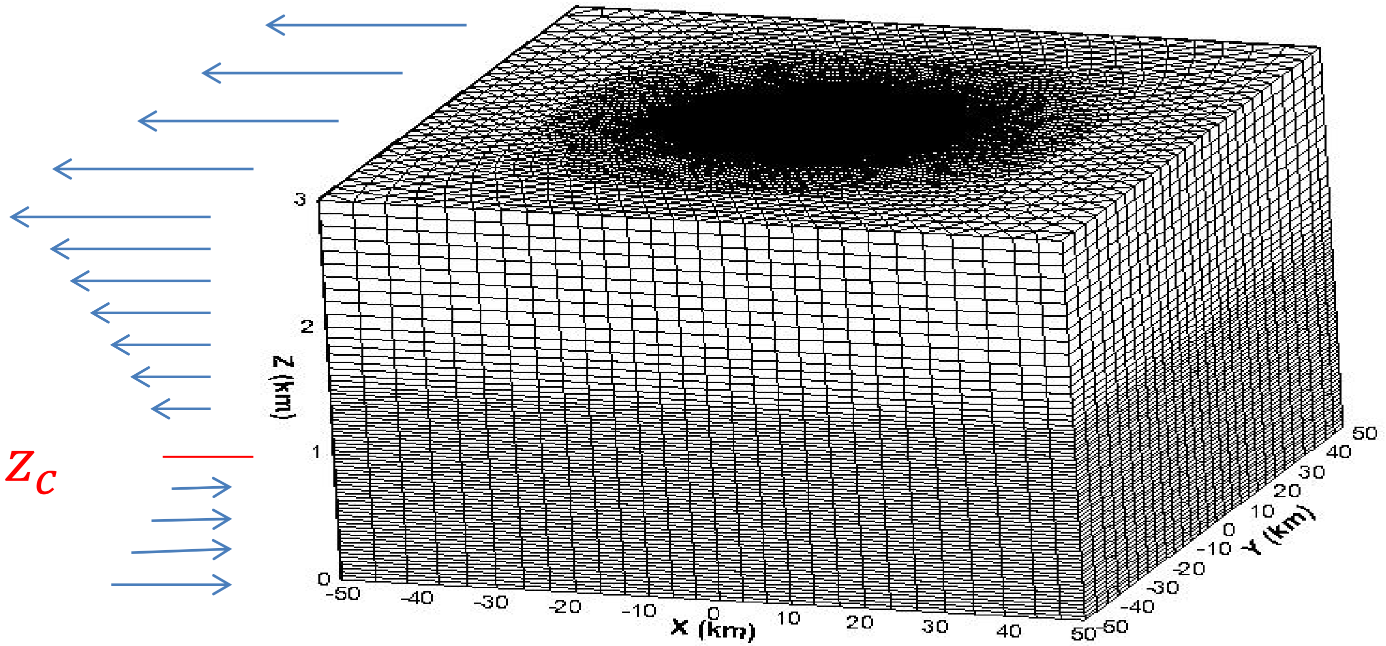

$$U_0 = 10\, ms^{-1}\,, \qquad U\left(z\right) = U_0\left(1 - \frac{z}{z_c}\right)$$

$$\frac{U_0}{N_a} = 0.2\,, \qquad R_i = \left(\frac{N z_c}{U_0}\right)^2 = 1\,, \qquad N = 0.01\, s^{-1}$$

$$a = 5000\, m\,, \qquad h(r) = h_0\left(1 + \frac{r^2}{a^2}\right)^{-\frac{3}{2}}\,, \qquad r \equiv \sqrt{x^2 + y^2}$$

Prismatic mesh

$$\tilde{z}_{i,k} = \tilde{z}_{i,k-1} + \delta\tilde{z}_k$$

$$\tilde{z}_{i,k} = \tilde{z}_{i,k}\left(1 - \frac{h_i}{H}\right) + h_i$$

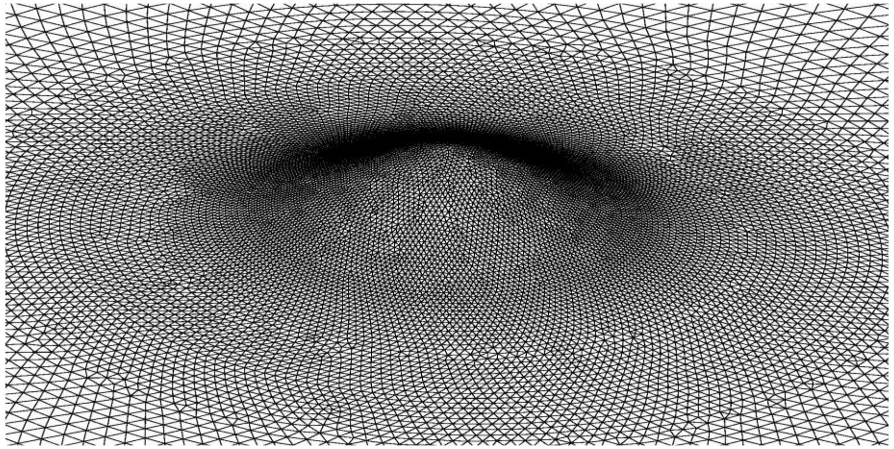

Triangular surface mesh

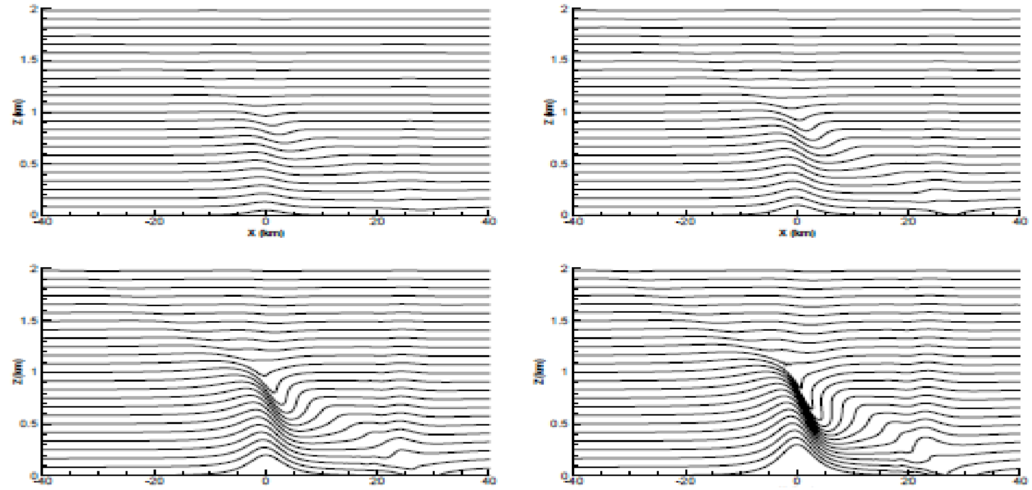

Fig. 12. Isentropes at T=6 in $y = 0$ vertical plane for experiments LS2 (left, top) LS3 (right, top), LS4 (left, bottom) and LS5 (right, bottom).

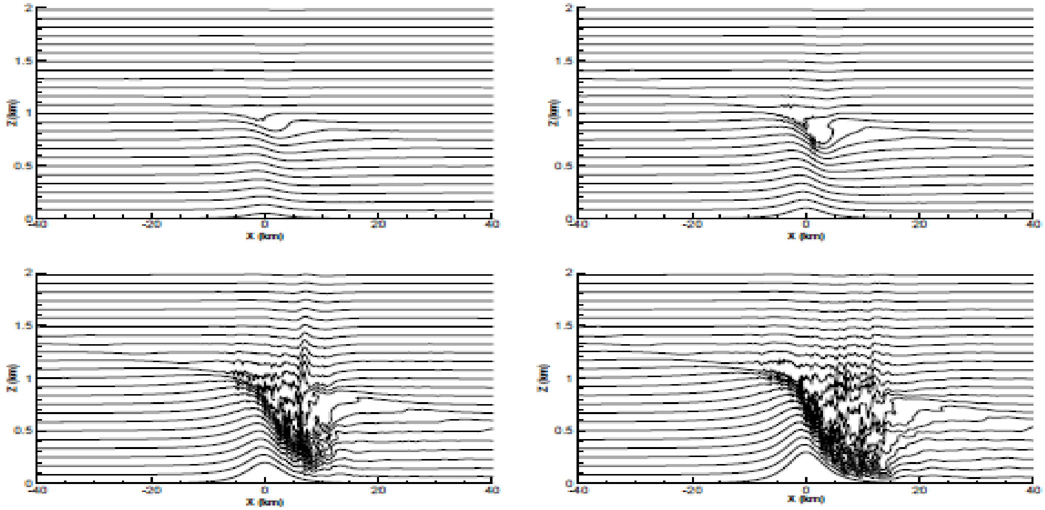

Fig. 13. As in Fig. 12 but at T=18.

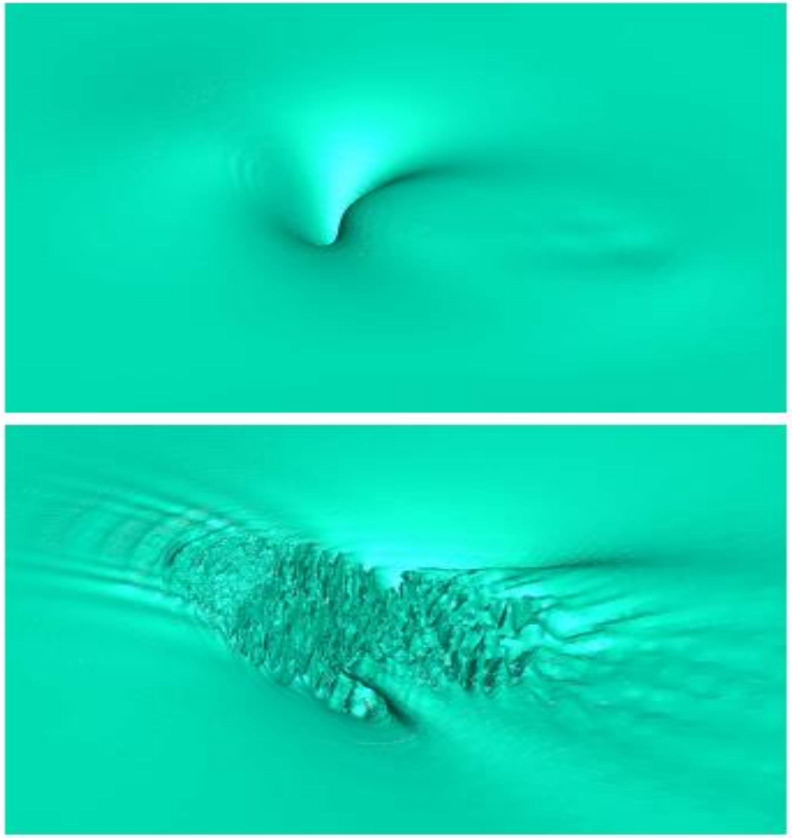

$T = 6$

$T = 18$

the isentrope with undisturbed height $z = 0.94 z_c$ LS5.

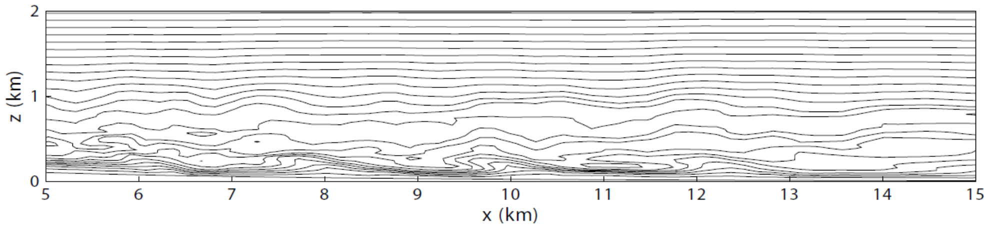

Stratified flows past a sphere

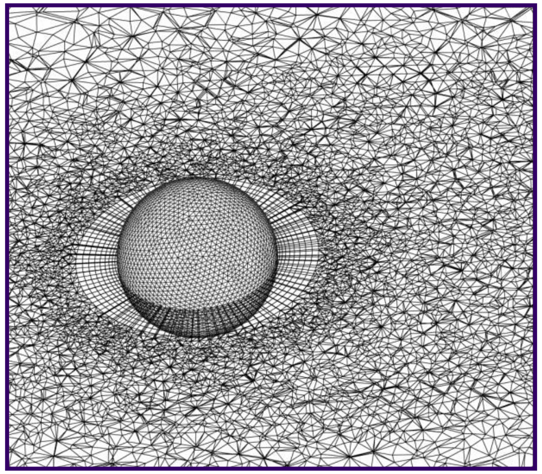

Cocetta et al. PoF 2021

$Re = 200$

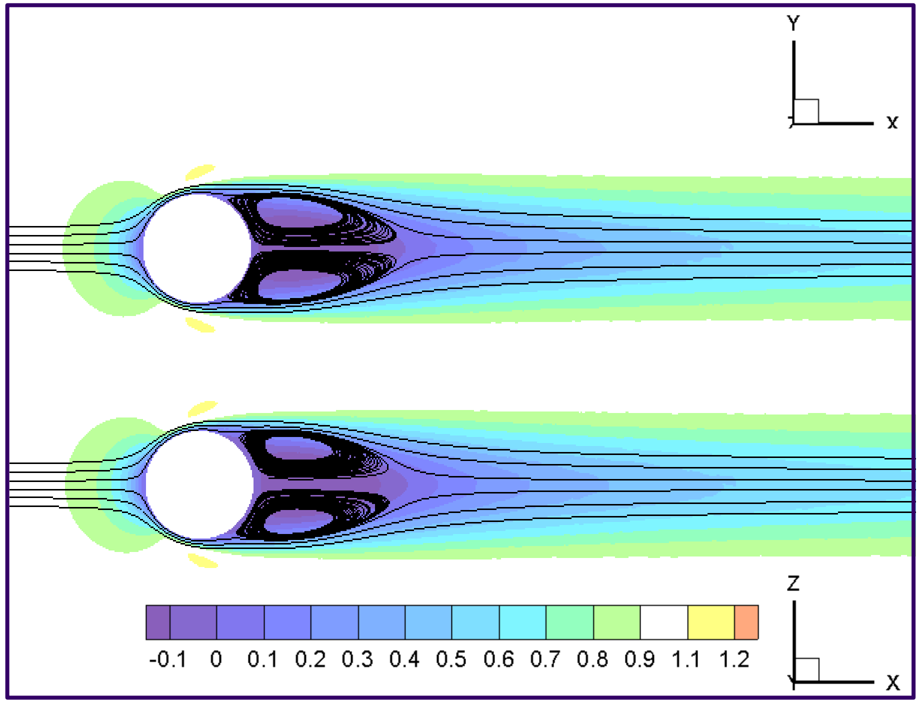

$Re = 300$

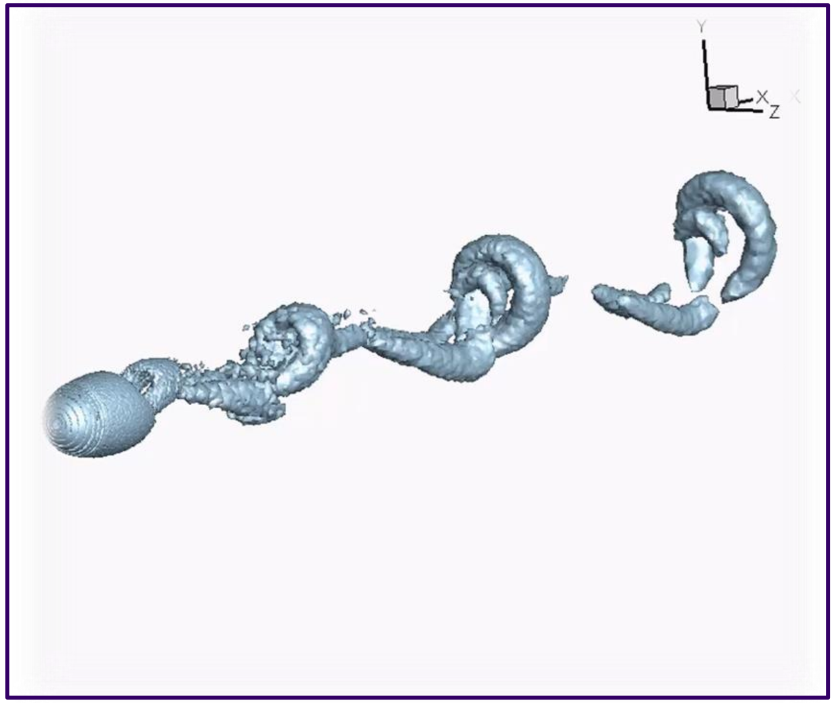

Q-method (second invariant of the deformation tensor)

Neutrally−stratified flow $Fr = \infty$

Non-axisymmetric attached vortex regime

$Fr = 2.5$

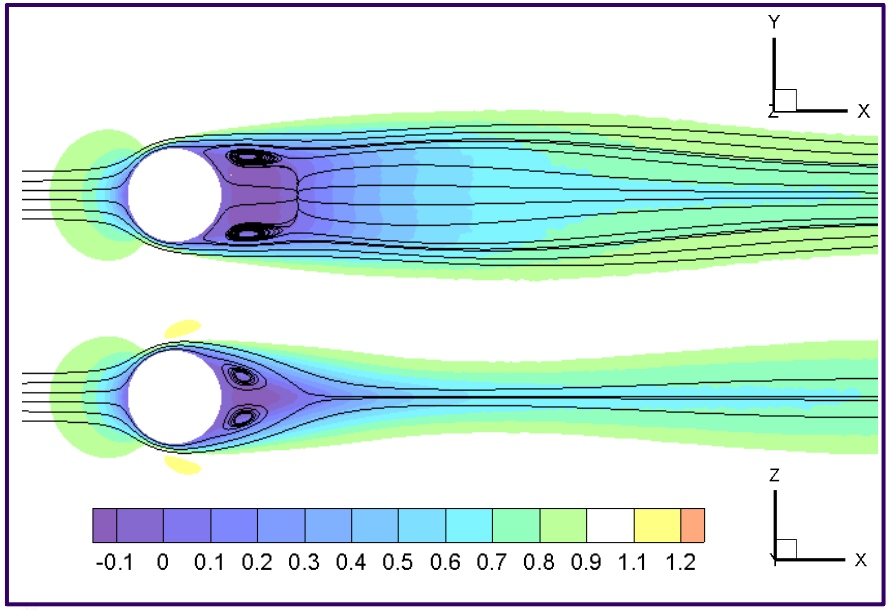

$Fr = 1.66$

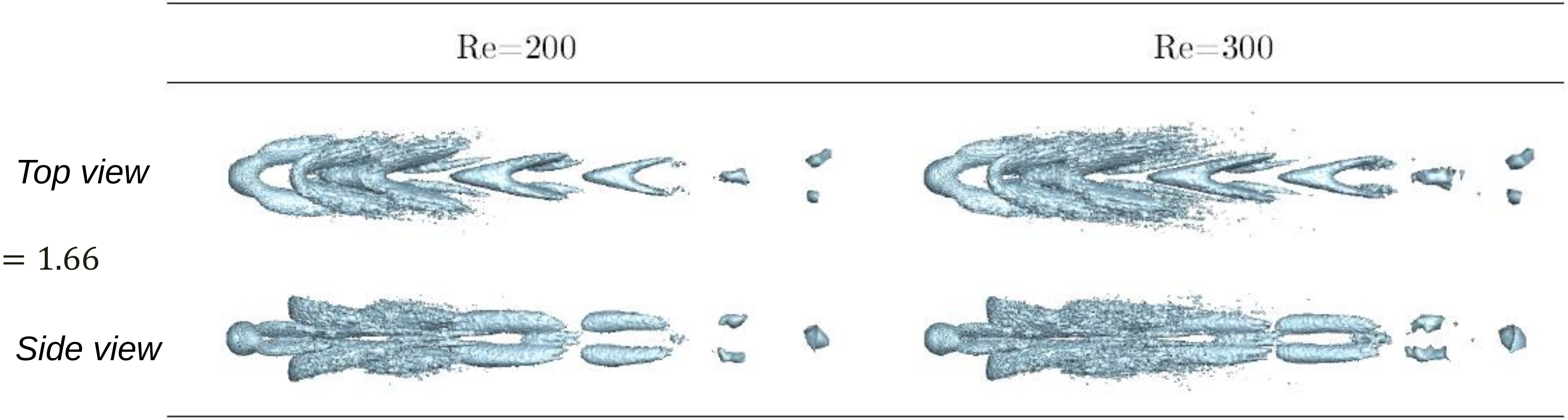

Lee-waves instability regime

$0.8 \gtrsim Fr \gtrsim 0.6$

$Re = 200$

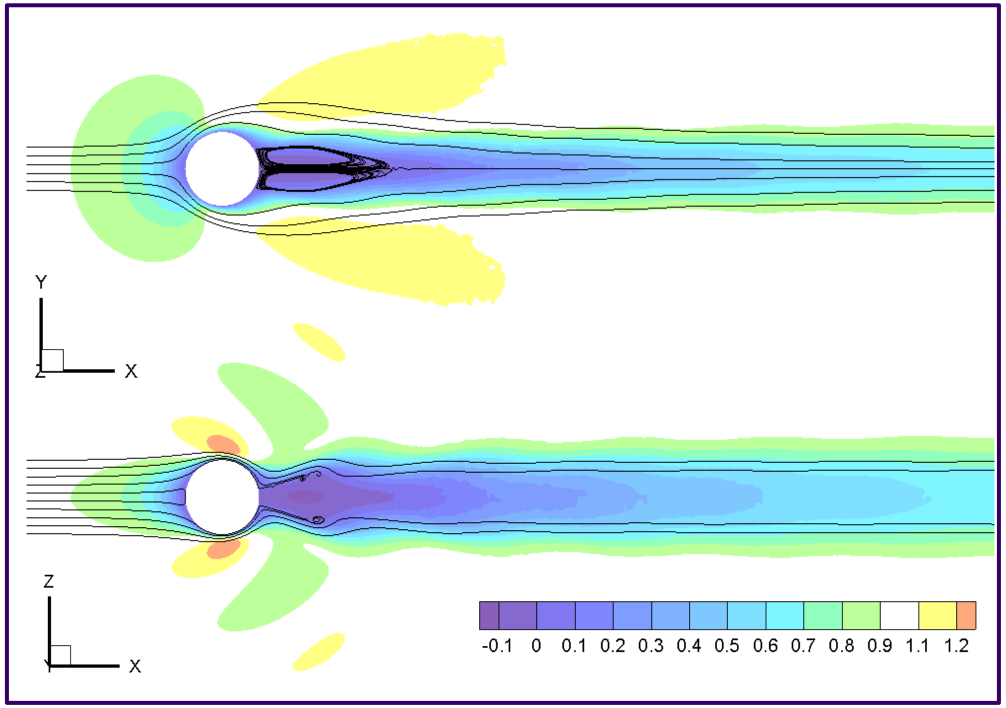

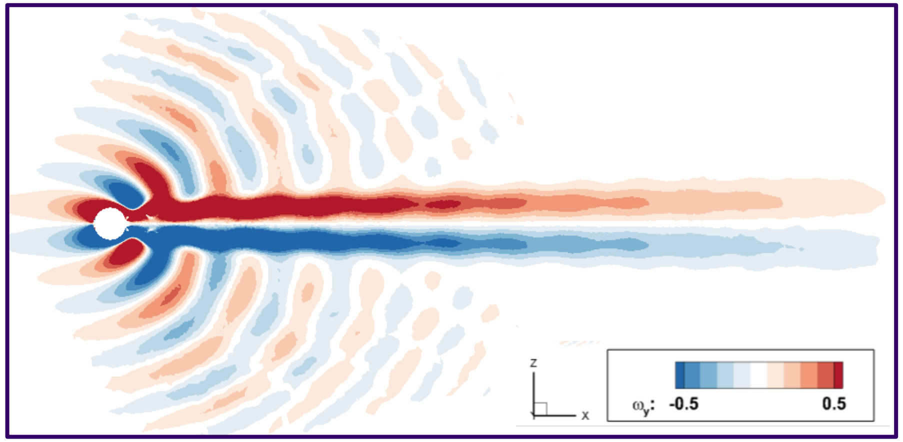

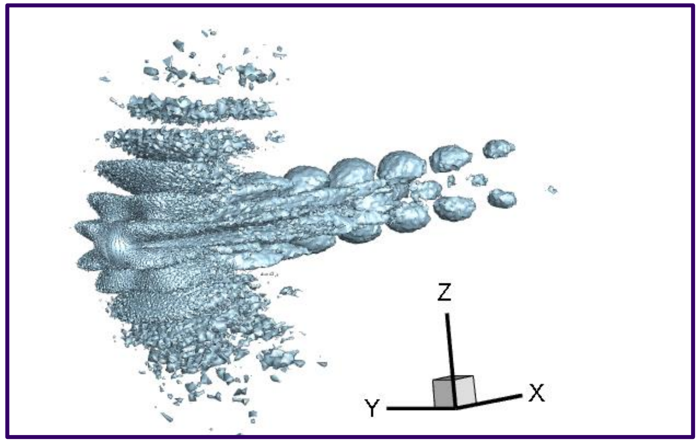

$Fr = 0.625$

Two-dimensional vortex shedding regime

$Fr \lesssim 0.6$

$Re = 200$

$Fr = 0.44$

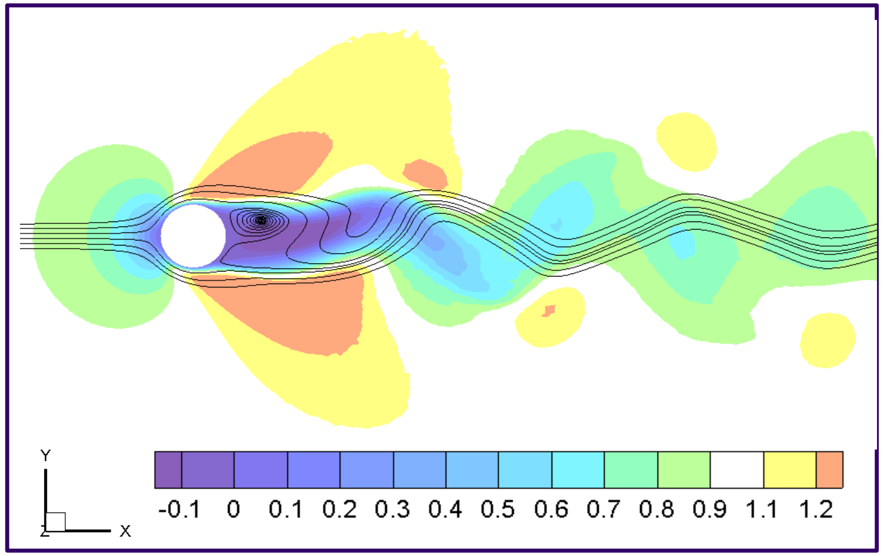

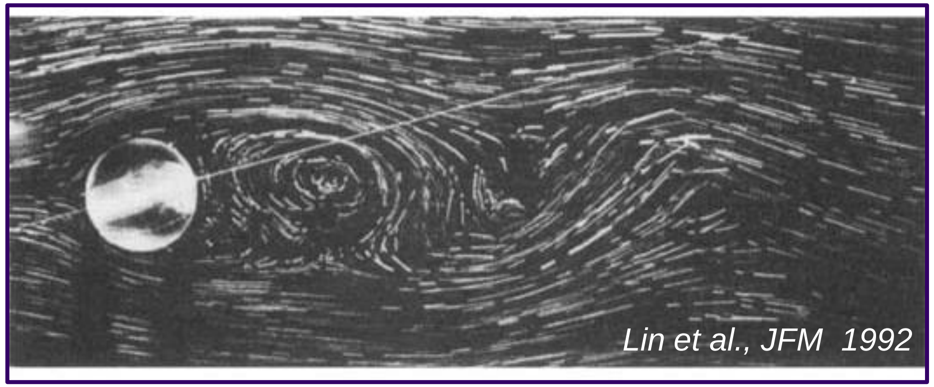

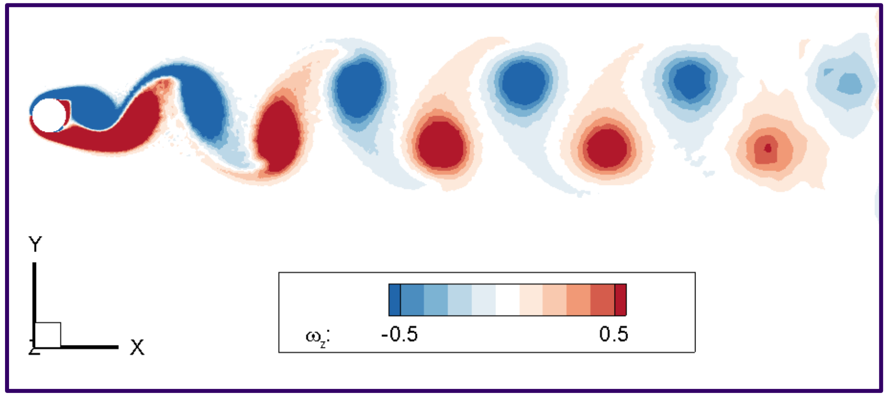

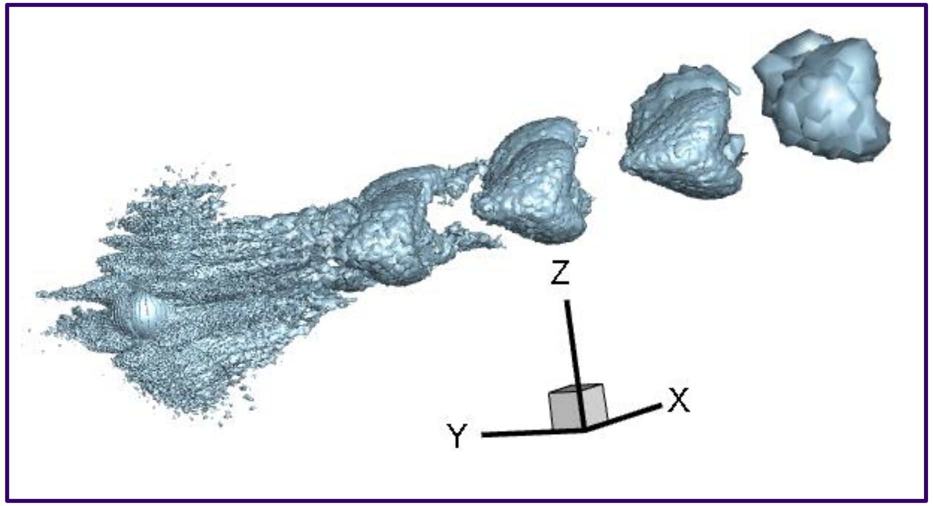

Study of drag coefficient

$Re = 200$

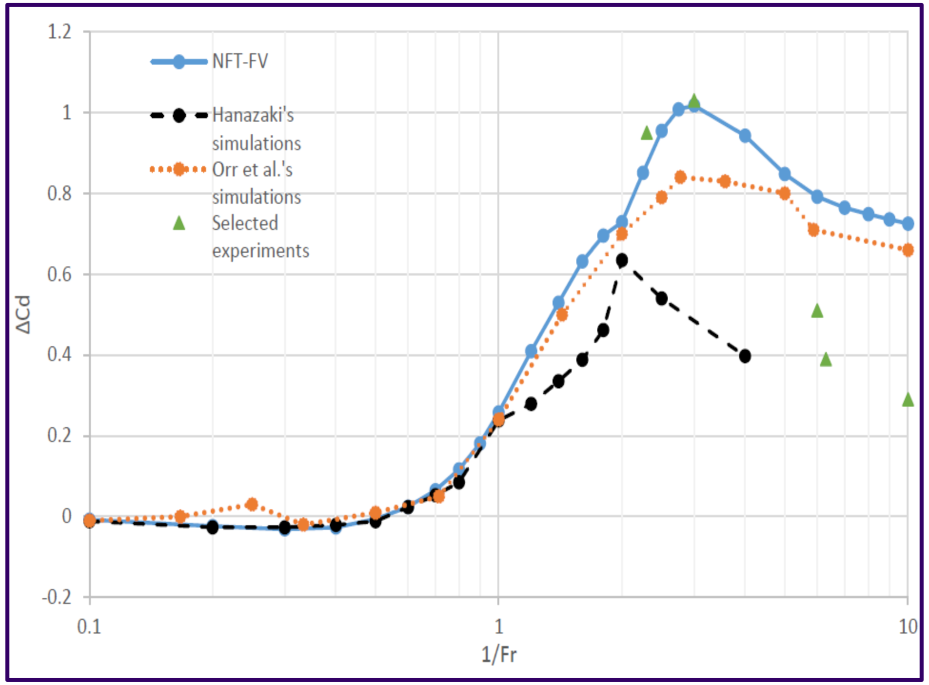

$Re = 300$

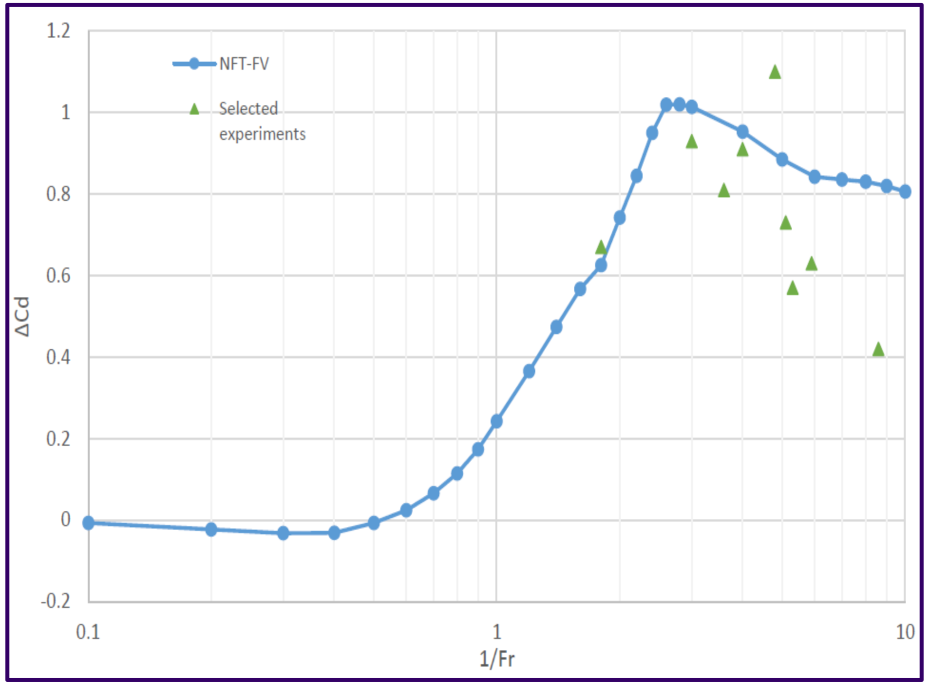

$$\Delta C_d = C_d(Re, {}^{1}/_{Fr}) - C_d(Re, 0)$$

$$C_d = \frac{F_d}{0.5\,\rho_o V_o^2 A}$$

Cocetta et al. PoF 2021

Stratified flow past two spheres

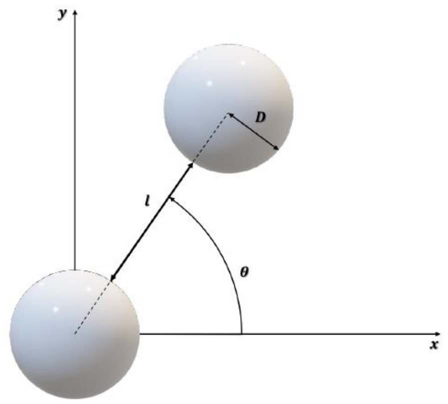

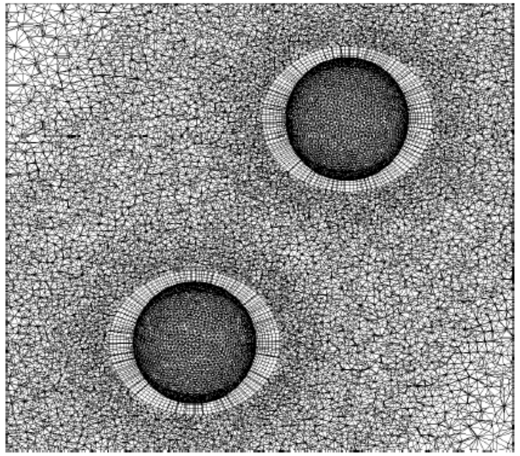

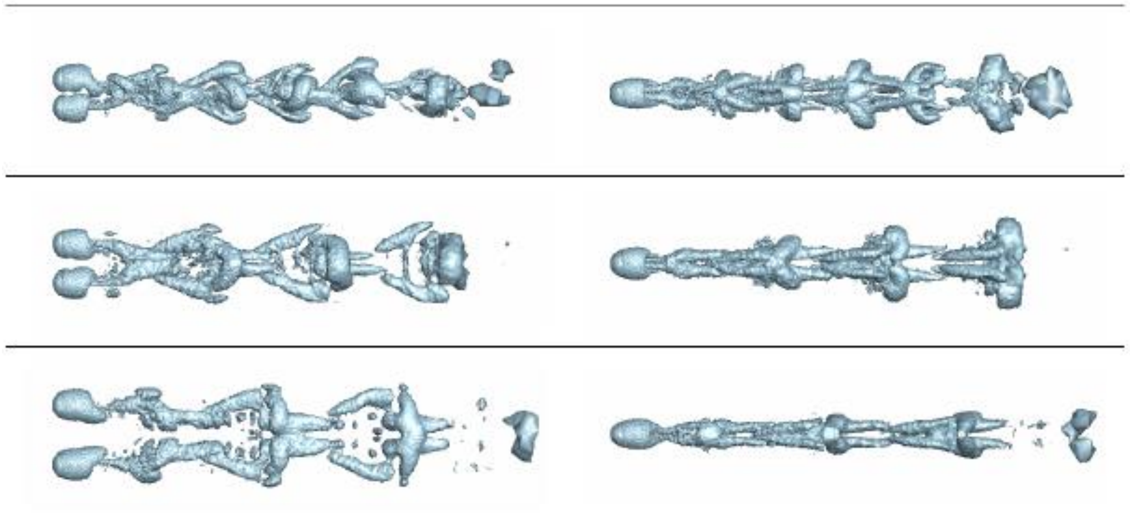

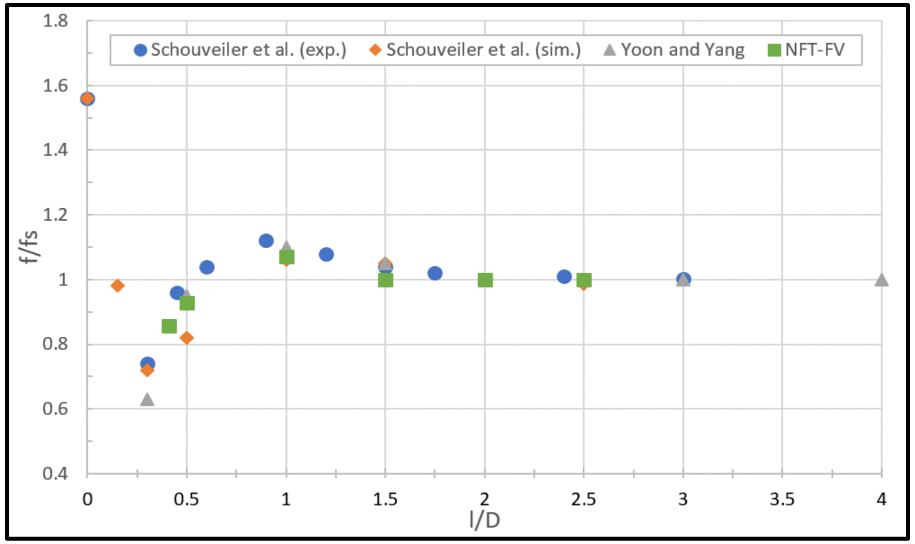

Top view *side view* *Re=300* *neutrally stratified*

Fr =1.625 steady-state non-axisymmetric attached vortex regime

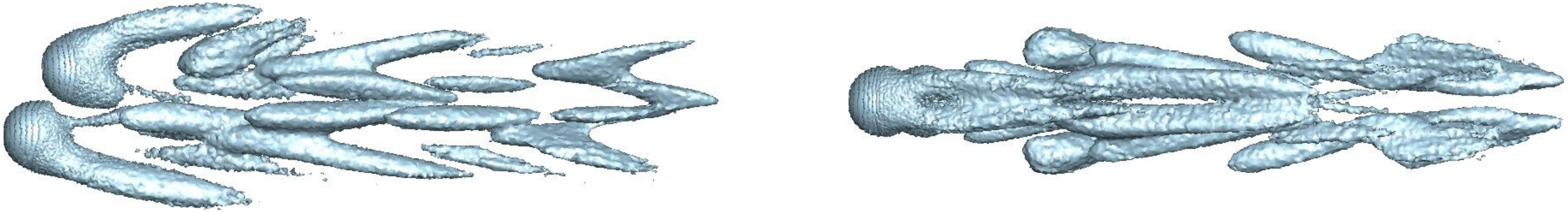

Fr=0.625 steady-state lee wave instability regime

Fr=0.25   two dimensional vortex shedding regime

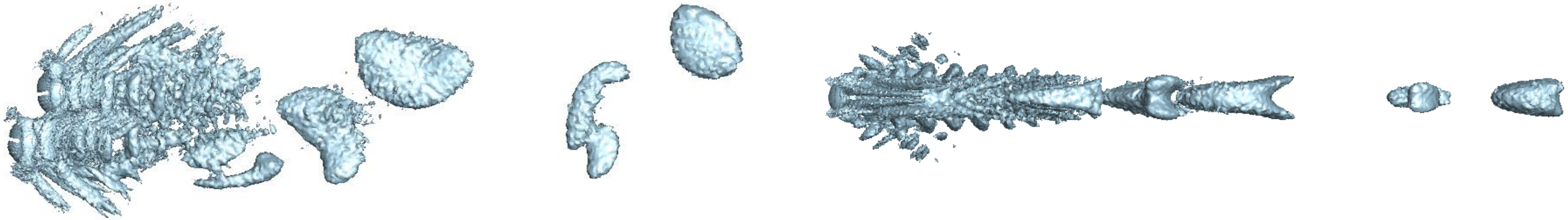

top view *side view*

Stratified flow past two spheres

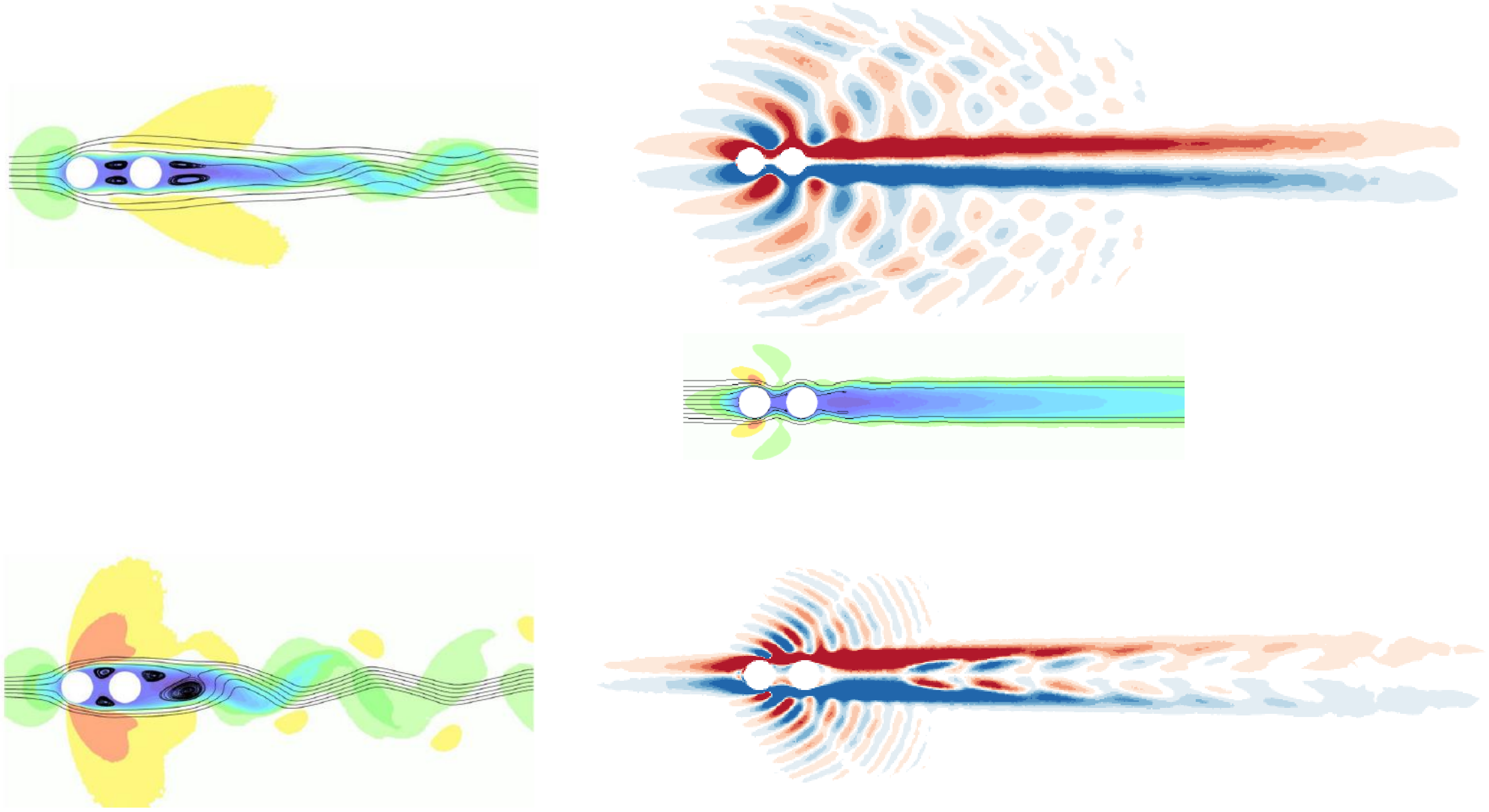

Fr=0.625

Fr=0.25

top view

side view

Remarks

- The presented NFT methodology can complement established NWP methods.

- Algorithmic parallel scalability is important for future computing architectures. Technical challenges of time to solution & energy efficiency have been partially addressed by a development of specialised preconditioners for the non-symmetric Krylov-subspace solver. For a global atmospheric model, the Jacobi preconditioning on a single mesh provides a substantial speed up.

- General characterisation of flows past spheres confirmed that stratification dominates the flow pattern for $Fr \searrow 0$ and unification of flow patterns. Flow patterns are sensitive to the spheres' relative location. Regimes characterising the flow past a single sphere are also observed for multi-sphere configurations.

- A record of consistent and accurate simulations for NFT MPDATA class of solvers continues to grow. Our recent developments targeted engineering applications and include a development of a LMN solver for strong thermally driven flows and implementation of the dynamic Smagorinski model.